

# High-Energy Al/CuO Nanocomposites Obtained by DNA-Directed Assembly

Fabrice Séverac, Pierre Alphonse, Alain Estève, Aurélien Bancaud,\* and Carole Rossi\*

Over the next few years, it is expected that new, energetic, multifunctional materials will be engineered. There is a need for new methods to assemble such materials from manufactured nanopowders. In this article, we demonstrate a DNA-directed assembly procedure to produce highly energetic nanocomposites by assembling Al and CuO nanoparticles into micrometer-sized particles of an Al/CuO nanocomposite, which has exquisite energetic performance in comparison with its physically mixed Al/CuO counterparts. Using 80 nm Al nanoparticles, the heat of reaction and the onset temperature are  $1.8 \text{ kJ g}^{-1}$  and  $410^\circ\text{C}$ , respectively. This experimental achievement relies on the development of simple and reliable protocols to disperse and sort metallic and metal oxide nanopowders in aqueous solution and the establishment of specific DNA surface-modification processes for Al and CuO nanoparticles. Overall, our work, which shows that DNA can be used as a structural material to assemble Al/Al, CuO/CuO and Al/CuO composite materials, opens a route for molecular engineering of the material on the nanoscale.

## 1. Introduction

Energetic materials store chemical energy that can be released upon thermal, electrical or optical actuation. These materials are the subject of intense research for military applications, as well as for civilian purposes, primarily including automotive air-bag propellants. Over the last decade, the idea of engineering molecularly built energetic materials with exquisite performance has launched the field of nanoenergetics.<sup>[1–3]</sup> Nanoparticles of aluminum are known to be one of the best nanoenergetic metals and for this reason they have been used in solid rocket motors. The metal of choice is aluminum because of its energy density, due to the high relative heat of formation of the oxide,  $\text{Al}_2\text{O}_3$ . New classes of nanoenergetic materials, in particular metastable intermolecular composites (MICs) or thermite nanocomposites, which are composed of oxidizer and fuel nanoparticles,

with typical particle sizes spanning tens to hundreds of nanometers, constitute a promising option for the development of propellants and explosives. So far MICs have been predominantly prepared by the physical mixing of powders, using aluminum nanoparticles (NPs) as the fuel and various oxidizers, including  $\text{MoO}_3$ , CuO,  $\text{Fe}_2\text{O}_3$  and  $\text{Bi}_2\text{O}_3$ .<sup>[4–9]</sup> These investigations established unambiguously that thermite-nanocomposite ignition and combustion properties can be affected by varying the size of the constituents and their intimacy.<sup>[4,5,7–16]</sup> For instance, decreasing the size of the nanoparticles enhances the combustion rate and lowers the ignition temperature. Moreover, the arrangement of the oxidizer and the fuel nanoparticles and their intimacy significantly impact the nanothermite burn rate and determine the propagation rate of the combustion wave front and the release of energy. As

a consequence, it has been demonstrated experimentally that having the maximum interfacial contact area between the oxidizer and the fuel is necessary to achieve optimal energetical performance. However, the preparation of a nanothermite by physical mixing does not allow the arrangement of the NPs to be controlled at the nanoscale.

Self-assembly techniques have been vaunted as a cutting-edge solution to precisely engineer the 3D organization of NPs and hence optimize the energetical properties of a nanothermite. Nanostructured composites have been, for instance, obtained by electrostatic self-assembly based on oppositely charging Al and  $\text{Fe}_2\text{O}_3$  NPs in aerosols<sup>[17]</sup> or by the functionalization of Al and CuO NPs with oppositely charged ligands.<sup>[18]</sup> Alternatively nanothermites composed of CuO nanorods and Al NPs have been assembled using poly(4-vinylpyridine) as the assembly material.<sup>[19]</sup> These different methods have allowed the generation of micrometer-sized nanothermites characterized by highly energetic performances. In another direction, DNA-directed assembly, which consists of coating two types of nanoparticles with single-stranded DNA molecules of complementary sequences, in order to direct the aggregation of NPs, has the unique potential to generate DNA-programmable NP crystals.<sup>[20]</sup> So far, this approach, which relies on the spontaneous formation of a DNA double helix held together by hydrogen bonds between complementary base pairs,<sup>[21,22]</sup> has mostly been performed with gold and silver NPs and applied to biodection or plasmonic applications.<sup>[20–24]</sup> While these NPs can be

Dr. F. Séverac, Dr. A. Estève, Dr. A. Bancaud, Dr. C. Rossi  
CNRS, LAAS, 7 Avenue du Colonel Roche, F-31077 Toulouse, France  
E-mail: rossi@laas.fr; abancaud@laas.fr

Dr. F. Séverac, Dr. A. Estève, Dr. A. Bancaud, Dr. C. Rossi  
Université de Toulouse  
UPS, INSA, INP, ISAE, LAAS, F-31077 Toulouse, France

Dr. P. Alphonse  
CIRIMAT, 118 Route de Narbonne,  
F-31062 Toulouse, France



DOI: 10.1002/adfm.201100763

considered to be well-defined model systems for fundamental research, the potential of DNA-directed assembly technology for other nanomaterials and applicative areas remains to be demonstrated and further explored.

In this paper, we add a new material to the already rich palette of applications of DNA-directed assembly technology by fabricating high-performance nanoenergetic materials. For this, specific approaches to disperse Al and CuO colloids from nanopowders are established, and different coating strategies with single-stranded DNA are validated. DNA-directed Al/CuO-nanocomposite assembly kinetics are then monitored in real time, and the intimacy of the NP arrangement in the resulting thermite nanocomposite is investigated using energy-dispersive X-ray (EDX) analysis. The energetic performances of the material in terms of onset temperature and heat of reaction are assessed quantitatively and compared to the literature, showing a significantly higher heat of reaction compared with physically and randomly mixed thermite nanocomposites.

## 2. Results and Discussion

The Al/CuO-nanocomposite assembly procedure is presented in Figure 1. CuO and Al NPs were purchased as solid powders, dispersed/sorted in an aqueous environment and functionalized with short single-stranded DNA molecules. These successive steps were first validated and the assembly of nanothermite was subsequently investigated.

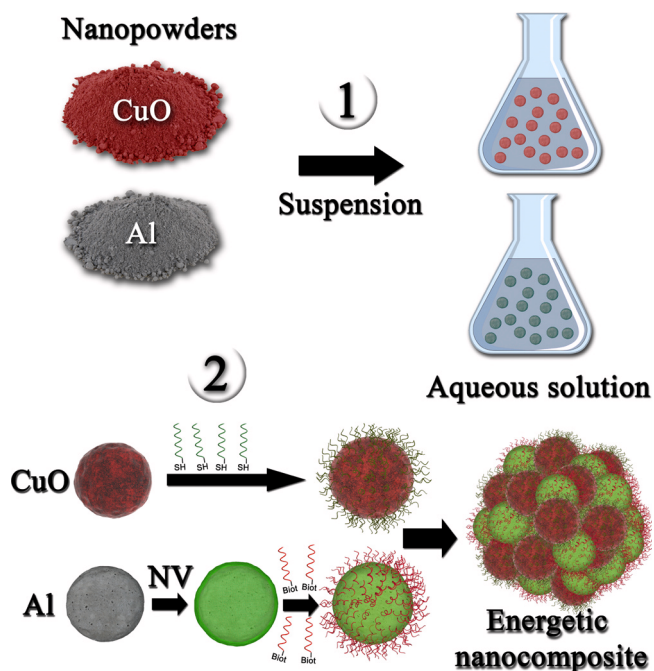


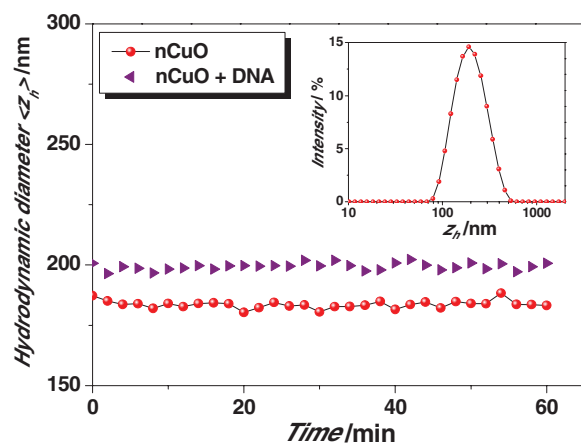
**Figure 1.** Schematic of the different steps for the DNA-directed assembly of the Al/CuO thermite nanocomposites. Aluminum and copper oxide nanopowders are first suspended and stabilized in aqueous solution, then functionalized with single DNA strands and eventually assembled through hybridization of the complementary DNA strands.

### 2.1. Dispersion and Surface Modification of Al and CuO Colloids

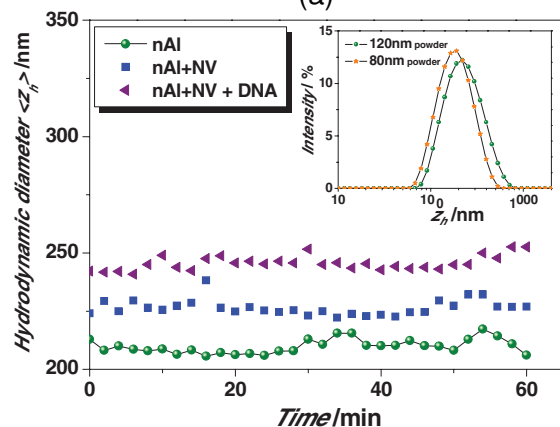
CuO powder, with a nominal size of 50 nm, and Al powder, with a nominal size of 80 nm or 120 nm, were dispersed in ultrapure water containing 0.1 % surfactant (polyoxyethylene (20) sorbitan monolaurate (Tween-20)) as a stabilization agent. These solutions were buffered at pH = 7 because copper oxide and aluminum oxide, which spontaneously forms a  $\approx 3$  nm passivation shell around Al NPs, are neither oxidized nor reduced in neutral conditions.<sup>[25,26]</sup> They were then sonicated for 3 min (see Experimental Section) in order to obtain colloidal solutions with mean hydrodynamic diameters of  $185 \pm 40$  nm,  $180 \pm 60$  nm and  $210 \pm 70$  nm for the 50 nm CuO, 80 nm Al and 120 nm Al NPs, respectively, as inferred from dynamic-light-scattering (DLS) experiments (inserts of Figure 2a,b). The resulting colloidal solutions were thus composed of small aggregates of  $\approx 2$ –4 NPs, as directly confirmed by scanning electron microscopy (SEM) (Figure S1, Supporting Information). These particles were stable in aqueous conditions over hours, as demonstrated by the constant hydrodynamic diameter derived from DLS (Figure 2a,b). Notably, we observed that longer periods of sonication did not reduce the size of these aggregates and, rather, produced colloidal suspensions of larger dimensions (Figure S2, Supporting Information).

The grafting strategy of the single-stranded DNA onto the CuO and Al NPs was first tackled by density-functional-theory (DFT) modeling. As in the well-known case of Au surfaces, thiol moieties, which are organosulfur compounds ( $-\text{SH}$ ), react with CuO surfaces to form Cu–S bonds, characterized by a gain in energy of  $-1.51$  eV; this is quantitatively even more favourable than in the case of Au–S bond formation, which is accompanied by an exothermic reaction pathway of  $-0.93$  eV. The grafting mechanism is associated with the intrinsic ability of CuO to be reduced by thiol moieties through the concomitant formation of sulfonic acids ( $-\text{SO}_3\text{H}$ ) or  $\text{H}_2\text{O}$  with exothermic energy budgets of  $-0.84$  and  $-1.27$  eV, respectively. These results are in keeping with protocols established for the formation of self-assembled monolayers on copper oxide surfaces.<sup>[27–30]</sup> The reducing properties of thiol moieties are no longer valid for oxidized aluminum, which exhibits an endothermic energy profile ( $+0.29$  eV). Consequently, two different strategies to graft single-stranded DNA onto CuO and Al NPs have to be developed.



On the one hand, the CuO NPs were functionalized with thiol-modified oligonucleotides (see Experimental Section), systematically showing a small increase in hydrodynamic diameter of  $\approx 10$  nm (Figure 2a). Given that the oligonucleotides measured 4 nm according to DLS measurements (data not shown), the presence of DNA at the surface of the NPs was expected to increase their hydrodynamic diameter by  $\approx 8$  nm, in keeping with our estimates. The surface modification of the CuO NPs with DNA was also confirmed by the detection of a change in surface potential of  $-9$  mV (table in Figure 2c). Finally, beyond the testimony of the successful modification of the CuO NPs with DNA, DLS measurements have provided direct evidence that the CuO colloids remain stable in water after DNA modification for at least 1 h (Figure 2a). On the other hand, the amphoteric nature of alumina surfaces and the high stability of its Al–O constituents led us to develop a strategy based on the non-specific binding of





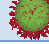
(a)



(b)

		Zeta-potential (mV)	Deviation
nCuO		-13	±5
nCuO + DNA		-22.4	±5.1

(c)

		Zeta-potential (mV)	Deviation
nAl		-22.6	±5.1
nAl + NV		-8.2	±5.7
nAl + NV + DNA		-23.1	±7.2

(d)

**Figure 2.** Stabilization and surface modification of the Al and CuO colloids. a) The average hydrodynamic diameter of the CuO nanoparticles suspended in aqueous solution before and after DNA functionalization (red and purple datasets, respectively) was measured using DLS. The inset shows the size distribution of the CuO colloid before surface modification. b) The average hydrodynamic diameter of the 120 nm Al nanoparticles suspended in aqueous solution after neutravidin coating and after DNA grafting (green, blue and purple datasets, respectively) was measured using DLS. The inset shows the size distribution of the 80 nm and the 120 nm Al colloids before surface modification (orange and green, respectively). c–d) The zeta potentials of the CuO and Al nanoparticles were measured at the different steps of the process.

neutravidin to aluminum oxide<sup>[31,32]</sup> (see details in the Experimental Section). Neutravidin is a tetrameric protein that forms one of the strongest non-covalent bonds with biotin, which is a small vitamin that can be coupled to virtually any biomolecule.<sup>[33]</sup> We observed that the adsorption of neutravidin to Al NPs induced a positive shift in the surface potential of +14 mV, together with an increase in the hydrodynamic diameter of 15 nm (Figure 2d and 2b). These two trends are consistent with the formation of a homogeneous protein layer because: i) neutravidin is a neutral protein at neutral pH, and ii) the diameter of avidin (a neutravidin analog) is  $\approx 7$  nm, according to X-ray crystallography.<sup>[34]</sup> We then added oligonucleotides chemically linked to biotin, which appeared to bind to the neutravidin-coated Al NPs, as inferred from the negative departure of the surface potential and the increase in the hydrodynamic diameter of 15 nm (Figure 2d and b). Given that we were dealing with NPs of similar size, the consistent zeta potentials for the DNA-coated Al and CuO NPs indicate that roughly similar DNA-grafting densities were reached for the two types of NP.

## 2.2. Assembly of CuO/CuO, Al/Al and Al/CuO Thermite Nanocomposites

Next, we focus on the mechanism of DNA-directed assembly of the Al and the CuO NPs. The aggregation kinetics, as inferred from the mean hydrodynamic diameter, were monitored in real time using DLS, and the pivotal role of DNA in the assembly was assayed by comparing the effect of complementary and non-complementary strands (for example ssA + ssB and ssA + ssC, respectively, in Table 1). The hydrodynamic diameters of the CuO/CuO, Al/Al and Al/CuO mixtures, which were mixed in stoichiometric ratios, remained constant over time at  $\approx 200$  nm with the non-complementary strands (lower datasets in Figure 3a–c). In contrast, the NPs coated with the complementary strands tended to aggregate, and CuO/CuO, Al/Al and Al/CuO nanocomposites of several micrometers were obtained within a few hours (upper datasets in Figure 3a–c), as confirmed by SEM images, which showed the existence of 1.9  $\mu\text{m}$ , compact Al/CuO aggregates composed of hundreds of individual Al

**Table 1.** List of DNA sequences; the complementary sequences are marked (see footnotes): sequence (a) could only hybridize with sequence (b) and sequence (c) could only hybridize with sequence (d).

DNA	Sequence (5' to 3')	Concentration
ssA	SH – (A) <sub>20</sub> CATACTGTACGTTAA <sup>a)</sup>	500 × 10 <sup>−6</sup> M
ssB	GTATGACATGCAATT <sup>b)</sup> (A) <sub>20</sub> – SH	500 × 10 <sup>−6</sup> M
ssC	TAACAATAATCCCTC <sup>c)</sup> (A) <sub>20</sub> – SH	500 × 10 <sup>−6</sup> M
ssA <sub>b</sub>	Biotin– (A) <sub>20</sub> CATACTGTACGTTAA <sup>a)</sup>	500 × 10 <sup>−6</sup> M
ssB <sub>b</sub>	GTATGACATGCAATT <sup>b)</sup> (A) <sub>20</sub> – Biotin	500 × 10 <sup>−6</sup> M
ssC <sub>b</sub>	TAACAATAATCCCTC <sup>c)</sup> (A) <sub>20</sub> – Biotin	500 × 10 <sup>−6</sup> M
Linker	GAGGGATTATTGTTA <sup>d)</sup> TTAACGTACAGTATG <sup>b)</sup>	500 × 10 <sup>−6</sup> M

a)Sequence (a); b)sequence (b); c)sequence (c); d)sequence (d).

and CuO NPs (Figure 4a). Moreover, the aggregation kinetics followed a non-linear temporal response, which was accurately fitted with a power-law function (solid lines in Figure 3a–c). Interestingly, the non-linear growth rates for the Al/Al, CuO/CuO and Al/CuO aggregates were characterized by exponents of  $0.57 \pm 0.01$ ,  $0.54 \pm 0.01$  and  $0.49 \pm 0.02$ , respectively. This scaling is consistent with the exponent of 0.56 observed for the formation of diffusion-limited aggregates,<sup>[35]</sup> which is obtained when the assembly dynamics are limited by NP diffusion. We then tested this interpretation by performing another experiment, in which the CuO and Al NPs were coated with non-complementary strands (ssA and ssC<sub>b</sub>). A linker, which was complementary to ssA and ssC<sub>b</sub> (Table 1), was subsequently added in excess to completely coat the surfaces of the Al and CuO NPs and impede the rapid formation of bridges between them, as in the mechanism of diffusion-limited aggregation. Note that bridges between the NPs eventually form because the association of the linker between the two ssA and ssC<sub>b</sub> strands is more stable thermodynamically. The assembly kinetics were expectedly slowed down (middle dataset in Figure 3c). Moreover, the aggregation growth rate became linear, this signature being characteristic of reaction-limited kinetics.<sup>[36]</sup> Consequently, our results demonstrate the successful fabrication of Al/CuO nanocomposites by DNA-directed assembly, and that the assembly kinetics can be monitored with different DNA-assembly strategies.

### 2.3. Characterization and Performance of DNA-Assembled Al/CuO Thermite Nanocomposites

The DNA-assembled Al/CuO thermite nanocomposites were subsequently analyzed at the individual aggregate level by EDX analysis in conjunction with SEM (Figure 4). The coarse-grained EDX energy spectrum of the cluster shown in Figure 4b indicates the presence of the NP structural elements, namely copper, aluminum and oxygen, as well as an expected peak due to phosphorus, due to the presence of DNA in the aggregates (Figure 4a). Thus, our assembly strategy enabled random aggregates of Al and CuO NPs to be obtained, and the the EDX spectrum qualitatively showed that Al and Cu were present in equivalent proportions of 33 % and 31 %, respectively (the percentages of the other atomic elements were 16 %, 5 %, 14 %

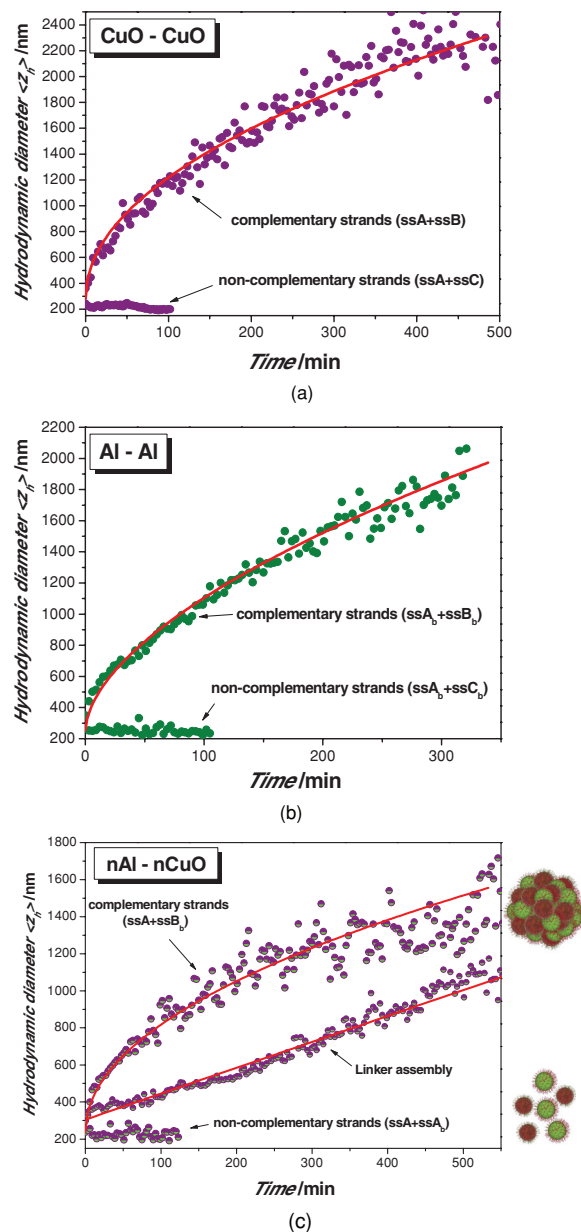


**Figure 3.** a–c) Real-time assembly kinetics of the Al and CuO nanoparticles. The mean hydrodynamic diameters of the DNA-coated CuO+CuO (a), Al+Al (b), and Al+CuO (c) colloidal solutions were monitored in real time, showing that aggregation did not occur with the non-complementary strands (lower datasets in each graph), and instantly started with the complementary oligonucleotides. The red lines represent fits of the kinetics with non-linear or linear temporal responses.

and 1 % for O, P, Ni and C, respectively). This result was further supported by mapping the presence of Al and Cu in individual clusters by performing spatially resolved EDX analysis (Figure S3, Supporting Information), which directly demonstrated the presence of Al and CuO NPs in the small aggregates. The thermal properties of the Al/CuO nanocomposites were then characterized by DSC (see Experimental Section). In a first set of experiments, the thermal decomposition of physically mixed and DNA-assembled Al/CuO nanocomposites



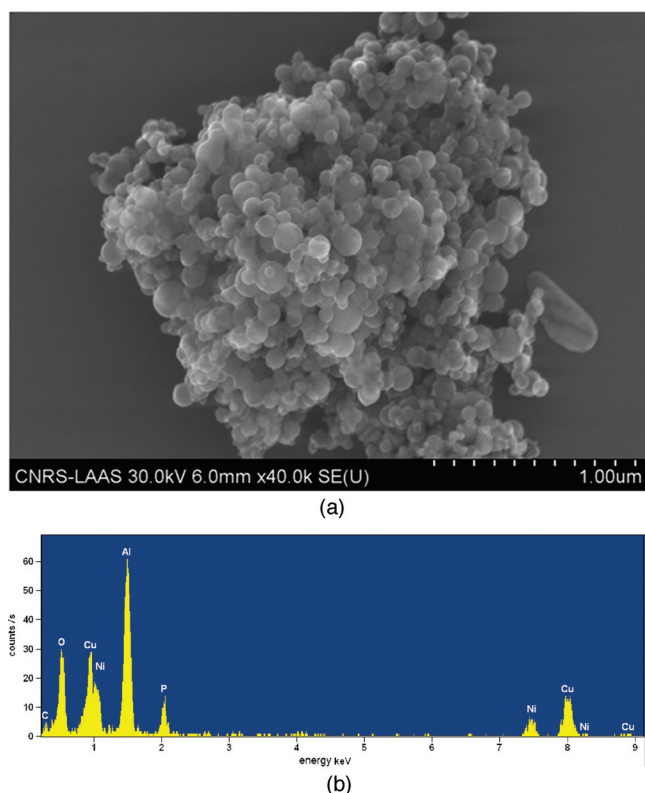


**Figure 4.** Structural characterization of the DNA-assembled Al/CuO thermite nanocomposites. a) SEM microscopy image of one individual Al/CuO aggregate of  $\approx 2 \mu\text{m}$ . b) The composition of the aggregate shown in (a) was investigated by EDX analysis, showing the presence of Al, Cu and O, as well as phosphorus (P) due to the presence of DNA in the aggregate. Note that carbon and nickel were also detected because of the use of carbon-coated nickel grids for the SEM imaging.

was compared (see **Figure 5**). The Al and CuO NPs were dispersed from the same commercial powders and stabilized in the same conditions (see Experimental Section), and both materials released heat upon thermal actuation. However, the heat of reaction was greatly enhanced for the DNA-assembled nanocomposites, as demonstrated by the total heat of reaction of  $1500 \text{ J g}^{-1}$  versus  $200 \text{ J g}^{-1}$ , starting from  $560^\circ\text{C}$  for the DNA-assembled nanothermite versus the physically mixed Al (120 nm)/CuO nanothermite, respectively (dashed areas in **Figure 5**). Notably, these heats of reaction are lower than the theoretical maximum of  $3900 \text{ J g}^{-1}$ , most likely because of the existence of a thin passivation oxide layer around the Al NPs,<sup>[37]</sup> as well as the presence of DNA at the interface between the Al and CuO. Nevertheless, we have clearly established that DNA-directed assembly of thermite nanocomposites results in an enhanced energy release. Next, we investigated whether the size of the Al NPs changed the onset temperature and the heat of reaction. The thermal decomposition of the DNA-assembled Al/CuO thermite nanocomposites made from the 120 nm and 80 nm Al NPs was compared using the same preparation protocols and stoichiometries. Integration of the exotherm indicated an increased total heat of reaction of  $1800 \text{ J g}^{-1}$  for the 80 nm Al NPs versus  $1500 \text{ J g}^{-1}$  for the 120 nm NPs. Interestingly, the measured heat of reaction ( $1800 \text{ J g}^{-1}$ ) and the

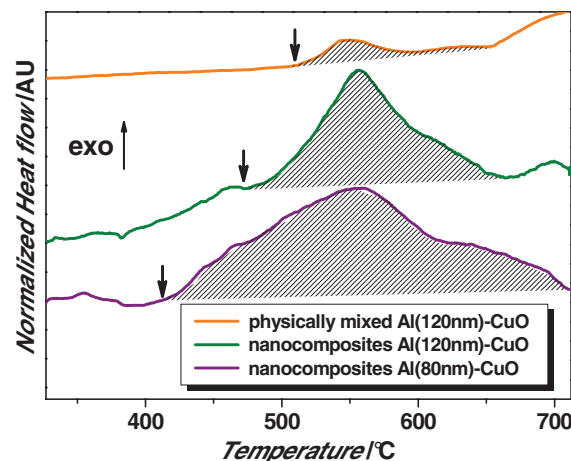


**Figure 5.** Energetic characterization of the Al/CuO nanocomposites. DSC curves of the Al/CuO aggregates produced by physical mixing of the Al (120 nm) and CuO nanoparticles (orange), DNA-directed assembly of Al (120 nm) and CuO nanoparticles (green), and DNA-directed assembly of Al (80 nm) and CuO NPs (purple). Note that the actual size of the Al nanoparticles differed from the specifications, as shown in **Figure 3b**. The heats of reaction were determined by the integration of the exotherm (hatched area), and the onset temperatures are indicated by vertical arrows. The DSC scans were performed at  $5 \text{ K min}^{-1}$  under a  $\text{N}_2$  atmosphere.

onset temperature ( $410^\circ\text{C}$ ) are among the best ever achieved for thermite nanocomposites. Indeed, maximal performances were obtained using an electrostatic NP assembly of Al and  $\text{Fe}_2\text{O}_3$ , yielding a comparable heat of reaction of  $1800 \text{ J g}^{-1}$ , which is 46 % of the theoretical value.<sup>[37]</sup> Our results also outperformed the results obtained by physically mixed Al/ $\text{MoO}_3$  nanothermite,<sup>[38]</sup> or by multilayered Al/CuO nanothermite,<sup>[39]</sup> both methods yielding a heat of reaction of  $1200 \text{ J g}^{-1}$ . We have also demonstrated that the onset temperature was reduced from  $470^\circ\text{C}$  to  $410^\circ\text{C}$  using the 80 nm Al NPs instead of the 120 nm NPs. Beyond the fact that this onset temperature is, to our knowledge, the lowest published in the literature, our results suggest that the ignition threshold can be tuned with Al NPs size while keeping the same assembly protocol. Interestingly this trend was also observed in earlier contributions, though based on drastic comparisons of Al nano- and micrometer-sized particles. For instance, a reduction of the ignition temperature from  $955^\circ\text{C}$  to  $476^\circ\text{C}$  was demonstrated with Al/ $\text{MoO}_3$  thermite composites containing 40 nm and  $10 \mu\text{m}$  Al particles, respectively.<sup>[6]</sup> These results are consistent with the onset temperature of  $460^\circ\text{C}$  measured for Al/ $\text{MoO}_3$  obtained with Al NPs of 52 nm.<sup>[38]</sup> In a similar direction, Granier and Pantoya examined the ignition sensitivity of thermite composites using Al nano- and micrometer-sized particles mechanically mixed with  $\text{MoO}_3$ <sup>[40]</sup> and demonstrated ignition-delay times two orders of magnitude lower for the thermite nanocomposites. Interestingly though, the ignition delay remained unchanged for Al NPs of 50 nm and 100 nm, using Al/CuO or Al/ $\text{MoO}_3$  nanothermites.<sup>[40,41]</sup>

The low level of the onset temperature obtained in our experiments may firstly be explained by the fact that Al NPs exhibit an increased surface energy associated with a reduced Al melting temperature, in comparison with large aluminum

particles.<sup>[42,43]</sup> When Al melts, the mechanism responsible for the ignition of nano-Al-based thermites is still speculated. One suggestion is that the expansion of the Al core upon heating breaks the alumina shell and leads to the ejection of small molten clusters of Al at a high velocity.<sup>[44]</sup> Another is the diffusion of Al atoms through physical cracks in the shell.<sup>[45,46]</sup> Apart from these still-controversial viewpoints, we also believe that the heterogeneous nature of our nanostructure is to be considered, since the DNA can provide a particular thermal signature. After the ignition threshold, the DSC curves are characterized by a gentle reaction profile, which indicates slow reaction kinetics. Moreover, it was clearly observed that the reaction kinetics were slower for the 80 nm NPs, compared with those of the 120 nm NPs. Interestingly, the presence of carbon on the DNA strands coating each NP may account for this lowering of the combustion rate and can also contribute to reducing the onset temperature. There is no certainty yet, but recent work by Siegert et al. has demonstrated that carbon nanofibers burn at 300 °C in contact with MnO<sub>2</sub>.<sup>[47]</sup> Moreover, in the same article, the authors measured a reduction of the combustion velocity from 730 mm s<sup>-1</sup> to 5 mm s<sup>-1</sup> by adding 37 % by weight of carbon nanofibers into the Al/MnO<sub>2</sub> nanothermite mixture, keeping the Al/MnO<sub>2</sub> weight ratio constant (50 %). It is also tempting to invoke that the potential concurrent reaction of Al with carbon (4Al + 3C → Al<sub>4</sub>C<sub>3</sub>) could contribute to the lowering of the reaction exothermicity.

### 3. Conclusions

This paper reports on the DNA-based, bottom-up nanofabrication of Al and CuO NPs into micrometer-sized particles of an Al/CuO thermite nanocomposite with an exquisite and tunable energetic performance in comparison with its physically mixed counterparts. This achievement has been reached owing to efforts to stabilize Al and CuO colloids obtained from commercial nanopowders in an aqueous environment. As validated by DFT calculations, two strategies were followed to bind oligonucleotides on Al and CuO NPs: thiol-modified oligonucleotides were attached to the copper oxide NPs and a biotin-neutravidin system was employed to the coat Al NPs. In the first case, the strong affinity of the thiol groups for copper oxide allowed the direct grafting of thiol-modified oligonucleotides to the CuO NPs. In the second case, neutravidin was adsorbed on the thin alumina shell covering the aluminum NPs, and biotin-modified oligonucleotides were grafted onto these protein-modified NPs. Micrometer-sized, self-assembled Al/CuO energetic nanocomposites were eventually obtained through DNA hybridization.

We characterized the resulting Al/CuO nanothermites using DSC, showing a total heat of reaction of 1800 J g<sup>-1</sup> for the 80 nm Al NPs, which is among the best ever achieved. We also demonstrated the possibility of tuning the onset temperature by changing the size of the aluminum NPs while keeping the same assembly protocol. Our methodological study, which has not yet provided the complete spectrum of characterizations (combustion velocity, ignition delay, etc.), to fully document the potential of DNA-assembled energetic materials and to reach an optimal performance, thus paves the way to a new route to fabricate nanothermites with precise control through the material-assembly reaction.

Interestingly, this strategy of assembling highly energetic nanothermite composites may enrich a number of applications in nanoenergetics, including environmentally clean primers, miniature safe detonators, thermal batteries, in situ welding, soldering and chemical-agent neutralization (i.e., thus-assembled nanothermite composites can be integrated in a portable apparatus to generate a high temperature (2000–3000 °C) for molecule degradation, applicable to neutralizing mustard agent, for example). Another possibility is to produce ions (Cu<sup>+</sup>, Al<sup>+</sup>, NO<sub>x</sub><sup>+</sup>) from the thermite reaction to provide effective pH control for local chemical neutralization, or specific chemical species could be also generated by grafting specific molecules with the nanothermite during the assembly process. On the longer term, we envisage that the DNA strands that direct the NP assembly could bear additional chemical, biological or physical cues to generate multifunctional energetic nanocomposites. For instance, the information encoded in the DNA strands may be exploited by incorporating specific sequences recognized by, for example, restriction enzymes<sup>[48]</sup> to trigger the irreversible dissociation of energetic materials for safely unloading fire devices. In another direction, absorbing dyes may be integrated into the DNA backbone in order to trigger energy release through light exposure. Finally, we posit that individual NPs can be functionalized with multiple DNA strands in order to assemble materials optimized to release heat, as well as, for example, gas for the generation of new propellants. Altogether DNA assembly thus appears to open new avenues towards the fabrication of multifunctional energetic materials.

### 4. Experimental Section

**Chemicals:** 50 nm copper oxide (CuO) and 120 nm or 80 nm aluminum (Al) nanopowders were purchased from PlasmaChem GmbH and Novacentrix, respectively. The Al NP purity was 75 %, from the manufacturer's data, leading to an alumina-shell thickness ranging from 3.3 to 5 nm (Figure S4, Supporting Information). All of the chemical reagents were purchased from Sigma-Aldrich and the oligonucleotides (Table 1) were purchased from Eurogentec. The DNA concentrations were systematically evaluated using UV-vis spectroscopy, using a Nanodrop 2000C spectrophotometer. All of the experiments were carried out with 1.5 mL hydrophobic microtubes to prevent unspecific adsorption on surfaces.

**Sonication:** 40 mg of the nanopowders were suspended in 50 mL of 0.1 M PBS + 0.1 % Tween-20, and the colloids were sonicated using a Vibra-Cell VCX 500 ultrasonic probe system at 200 W for 3 min, with 2 s pulses separated by 1 s. Notably, the Tween-20 surfactant was selected because it does not interfere with the interaction properties of biomolecules, and, in particular, with the biotin-streptavidin binding reaction.

**DLS and Zeta-Potential Measurements:** A Zetasizer Nano ZS instrument (Malvern Instruments) was used to determine the NP hydrodynamic diameter by DLS and the zeta potential by Doppler laser electrophoresis. All of the zeta-potential measurements were performed in water, and the temperature was maintained at 25 °C.

**SEM:** The samples were thoroughly rinsed 5 times with a volatile salt (20 × 10<sup>-3</sup> M ammonium acetate) before SEM imaging, which was performed on a Hitachi S4800 instrument coupled to an EDX-spectroscopy system. The samples were prepared by depositing and evaporating a droplet of the aqueous colloidal solution on a carbon-coated nickel grid.

**DSC:** DSC measurements were performed on a SETARAM DSC 111G system under nitrogen flow with a Supelco super-clean gas-purifier oxygen trap over the temperature range from 300 K to 1000 K and at a heating rate of 5 K min<sup>-1</sup>. The samples were transferred and evaporated in an alumina crucible for thermal analysis.

**Preparation of the DNA-Modified CuO NPs:** The terminal sulfur atoms of the thiolated DNA molecules tend to form dimers in solution. Prior to use, thiolated DNAs were thus deprotected by cleaving the disulfide bonds using 0.1 M of dithiothreitol (DTT) dissolved in phosphate buffered saline (PBS) over a period of 1 h. The DTT was then removed using a desalting NAP-5 column (GE Healthcare), and the freshly deprotected thiolated oligonucleotides were added to the CuO colloid at a final concentration of  $3 \times 10^{-6}$  M. This mixture was left overnight on a microtube rotator to prevent sedimentation. The solution was then buffered to  $10 \times 10^{-3}$  M phosphate ( $\text{NaH}_2\text{PO}_4/\text{Na}_2\text{HPO}_4$ ) and to 0.1 M NaCl by dropwise addition of a 2 M NaCl solution. After 24 h, excess DNA was eventually removed by multiple centrifugations at 14 000 rpm (5 min), and the NPs were resuspended in 0.3 M PBS to conduct the assembly experiments.

**Preparation of the DNA-Modified Al NPs:** 6  $\mu\text{L}$  of neutravidin ( $1 \text{ mg mL}^{-1}$ ) was added to 1 mL of sonicated Al NPs over 30 min. The excess reagent was removed by 5 centrifugations at 14 000 rpm (5 min), and the neutravidin-coated NPs were resuspended in 0.1 M PBS. Then, biotin-modified oligonucleotides were added at a final concentration of  $3 \times 10^{-6}$  M and allowed to stand for 2 h on the microtube rotator. The DNA-coated NPs were eventually rinsed, as described for the CuO NPs, with 0.3 M PBS. Interestingly, we noted that the Al NPs were stable in 0.3 M PBS + 0.1 % Tween-20 over a period of weeks, whereas the particles were oxidized in a few days when dispersed in ultrapure water.

**Preparation of the Physically Mixed Al-CuO Composites:** 40 mg of unmodified 120 nm Al and CuO nanopowders were suspended in 50 mL of ultrapure water supplemented with 0.1 % Tween-20. This mixture was then suspended using ultrasonic waves over 3 min, as described in the Sonication part of Experimental Section.

## Supporting Information

Supporting Information is available from the Wiley Online Library or from the author.

## Acknowledgements

This work was supported in part by the French Defence Agency (DGA). We are grateful to have been granted access to the bionanotechnologies platform at ITAV-UMS3039 and to its DLS equipment. We thank Ayse Berber a DGA PhD student for her advise.

Received: April 6, 2011

Revised: June 13, 2011

Published online: October 18, 2011

- [1] A. W. Miziolek, *The AMPTIAC Newsletter* **2002**, 6, No. 1.
- [2] S. F. Son, R. Yetter, Y. Yang, *J. Propulsion Power* **2007**, 23, 643.
- [3] C. Rossi, A. Estève, P. Vashishta, *J. Phys. Chem. Solids* **2010**, 71, 57.
- [4] B. S. Bockmon, M. L. Pantoya, S. F. Son, B. W. Asay, J. T. Mang, *J. Appl. Phys.* **2005**, 98, 064903.
- [5] T. Foley, A. Pacheco, J. Malchi, R. Yetter, K. Higa, *Propellants, Explos., Pyrotech.* **2007**, 32, 431.
- [6] M. L. Pantoya, J. J. Granier, *J. Therm. Anal. Calorimetry* **2006**, 85, 37.
- [7] E. V. Sanders, B. W. Asay, T. Foley, B. C. Tappan, A. Pacheco, S. F. Son, *J. Propulsion Power* **2007**, 23, 8.
- [8] M. Schoenitz, S. Umbrajkar, E. Dreizin, *J. Propulsion Power* **2007**, 23, 5.
- [9] S. F. Son, B. W. Asay, T. Foley, R. Yetter, M. Wu, G. Risha, *J. Propulsion Power* **2007**, 23, 7.
- [10] R. Armstrong, N. Thadhani, W. Wilson, J. Gilman, R. E. Simpson, *Mater. Res. Soc. Symp. Proc.* **2003**, 800.
- [11] C. E. Aumann, G. L. Skofronick, J. A. Martin, *The 3rd Int. Conf. Nanometer-Scale Sci. Technol.* **1995**, 13, 1178.
- [12] S. H. Fischer, M. C. Grubelich, *AIAA Meeting paper on Disc* **1996**, 1.
- [13] M. L. Pantoya, J. J. Granier, *Propellants, Explosives, Pyrotechnics* **2005**, 30, 53.
- [14] J. A. Puszynski, C. J. Bulian, J. J. Swiatkiewicz, *J. Propulsion Power* **2007**, 23, 9.
- [15] N. Thadhani, R. Armstrong, A. Gash, W. E. Wilson, *Mater. Res. Soc. Symp. Proc.* **2006**, 57.
- [16] K. C. Walter, D. R. Pesiri, D. E. Wilson, *J. Propulsion Power* **2007**, 23, 6.
- [17] S. H. Kim, M. R. Zachariah, *Adv. Mater.* **2004**, 16, 1821.
- [18] J. Y. Malchi, T. J. Foley, R. A. Yetter, *ACS Appl. Mater. Interfaces* **2009**, 1, 2420.
- [19] R. Shende, S. Subramanian, S. Hasan, S. Apperson, R. Thiruvengadathan, K. Gangopadhyay, S. Gangopadhyay, P. Redner, D. Kapoor, S. Nicolich, W. Balas, *Propellants, Explos., Pyrotech.* **2008**, 33, 239.
- [20] S. Y. Park, A. K. R. Lytton-Jean, B. Lee, S. Weigand, G. C. Schatz, C. A. Mirkin, *Nature* **2008**, 451, 553.
- [21] C. A. Mirkin, *Inorg. Chem.* **2000**, 39, 2258.
- [22] C. A. Mirkin, R. L. Letsinger, R. C. Mucic, J. J. Storhoff, *Nature* **1996**, 382, 607.
- [23] R. C. Mucic, J. J. Storhoff, C. A. Mirkin, R. L. Letsinger, *J. Am. Chem. Soc.* **1998**, 120, 12674.
- [24] C. J. Loweth, W. B. Caldwell, X. Peng, A. P. Alivisatos, P. G. Schultz, *Angew. Chem. Int. Ed.* **1999**, 38, 1808.
- [25] T. Hagyard, J. R. Williams, *Trans. Faraday Soc.* **1961**, 57, 2288.
- [26] R. S. Alwitt, J. W. Dekker, in *Oxides and Oxide Films*, Vol. 4, (Ed: J. W. Diggel), Marcel Dekker, New York **1976**, p. 169.
- [27] D. L. Allara, R. G. Nuzzo, *Langmuir* **1985**, 1, 52.
- [28] D. L. Allara, R. G. Nuzzo, *Langmuir* **1985**, 1, 45.
- [29] J. P. Folkers, C. B. Gorman, P. E. Laibinis, S. Buchholz, G. M. Whitesides, R. G. Nuzzo, *Langmuir* **1995**, 11, 813.
- [30] P. E. Laibinis, G. M. Whitesides, D. L. Allara, Y. T. Tao, A. N. Parikh, R. G. Nuzzo, *J. Am. Chem. Soc.* **1991**, 113, 7152.
- [31] J. Korlach, P. J. Marks, R. L. Cicero, J. J. Gray, D. L. Murphy, D. B. Roitman, T. T. Pham, G. A. Otto, M. Foquet, S. W. Turner, *Proc. Natl. Acad. Sci. USA* **2008**, 105, 1176.
- [32] H. Susmita, D. K. Chattoraj, *Indian J. Biochem. Biophys.* **1991**, 28, 114.
- [33] E. P. Diamandis, T. K. Christopoulos, *Clin. Chem.* **1991**, 37, 625.
- [34] J. A. E. Määttä, T. T. Airenne, H. R. Nordlund, J. Jänis, T. A. Paldanius, P. Vainiotalo, M. S. Johnson, M. S. Kulomaa, V. P. Hytönen, *ChemBioChem* **2008**, 9, 1124.
- [35] D. A. Weitz, J. S. Huang, M. Y. Lin, J. Sung, *Phys. Rev. Lett.* **1984**, 53, 1657.
- [36] S. Cobbe, S. Connolly, D. Ryan, L. Nagle, R. Eritja, D. Fitzmaurice, *J. Phys. Chem. B* **2002**, 107, 470.
- [37] S. H. Fischer, M. C. Grubelich, *Proc. 24th Int. Pyrotech. Seminar, Monterey, CA, USA 27–31 July 1998*, International Pyrotechnics Society, **1998**, 231.
- [38] J. Sun, M. L. Pantoya, S. L. Simon, *Thermochim. Acta* **2006**, 444, 117.
- [39] M. Petrantonio, C. Rossi, L. Salvagnac, V. Conedera, A. Esteve, C. Tenaillon, P. Alphonse, Y. J. Chabal, *J. Appl. Phys.* **2010**, 108, 084323.
- [40] J. J. Granier, M. L. Pantoya, *Combust. Flame* **2004**, 138, 373.
- [41] C. J. Bulian, T. Kerr, J. A. Puszynski, *Proc. 31st Int. Pyrotech. Seminar, Fort Collins, CO, USA 11–16 July, 2004*, International Pyrotechnics Society, **2004**, 327.
- [42] J. Eckert, J. C. Holzer, C. C. Ahn, Z. Fu, W. L. Johnson, *Nanostruct. Mater.* **1993**, 2, 407.
- [43] C. R. M. Wronski, *Br. J. Appl. Phys.* **1967**, 18, 1731.
- [44] V. I. Levistas, B. W. Asay, S. F. Son, M. Pantoya, *J. Appl. Phys.* **2007**, 101, 083524.
- [45] A. Rai, K. Park, L. Zhou, M. R. Zachariah, *Combust. Theory Modelling* **2006**, 10, 843.
- [46] B. J. Henz, T. Hawa, M. R. Zacharia, *J. Appl. Phys.* **2010**, 107, 024910.
- [47] B. Siegert, M. Comet, O. Muller, G. Pourroy, D. Spitzer, *J. Phys. Chem.* **2010**, 114, 19562.
- [48] A. G. Kanaras, Z. Wang, A. D. Bates, R. Cosstick, M. Brust, *Angew. Chem.* **2003**, 115, 201.